ACS Catalysis

pubs.acs.org/acscatalysis
Research Article

Hollow $Au_1Cu_1(111)$ Bimetallic Catalyst Promotes the Selective Electrochemical Conversion of Glycerol into Glycolic Acid

Lingqin Shen, Luyao Sun, Mark Douthwaite, Ouardia Akdim,* Stuart Taylor, and Graham J. Hutchings*

Cite This: *ACS Catal.* 2024, 14, 11343−11351
Read Online

ACCESS | Metrics & More | Article Recommendations | Supporting Information

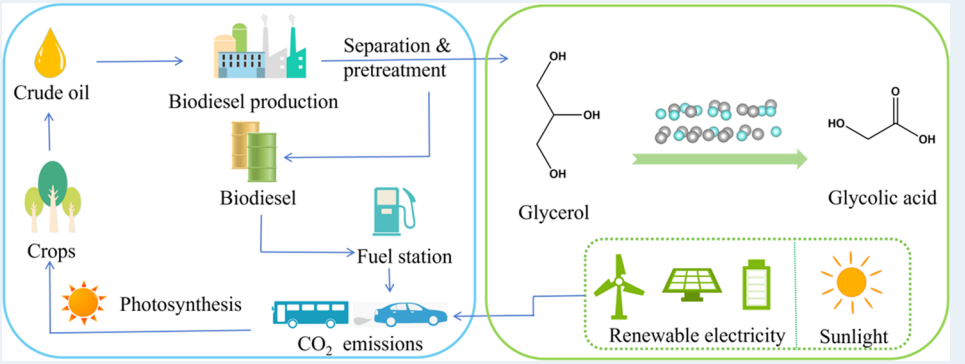

ABSTRACT: Electrochemical catalysis of polyols enables precise control over the cleavage of C−C and C−O bonds, facilitating high selectivity toward high-value glycolic acid. Here, we report that a hollow spheroidal bimetallic Au_1Cu_1 catalyst demonstrates high activity and selectivity toward glycerol, 1,2-propanediol, and ethylene glycol electrooxidation. Under the optimized conditions, glycerol conversion and glycolic acid selectivity reached 90 and 45%, respectively. The Au_1Cu_1 catalyst exhibits good stability after multiple cycles of electrolysis. Structural characterization and density functional theory (DFT) calculations confirmed that the hollow structure of the catalyst enhances the electrochemical surface area, with the $Au_1Cu_1(111)$ facet facilitating the selective electrocatalytic conversion of glycerol to glycolic acid.

KEYWORDS: *glycerol electrooxidation, glycolic acid, $Au_1Cu_1(111)$, DFT, electrocatalysis*

INTRODUCTION

The utilization of biomass as a feedstock for producing high-value chemicals has garnered significant interest in recent years, driven by the growing global energy demand and related environmental issues.[1−3] Polyols, such as glycerol, 1,2-propanediol, and ethylene glycol, are particularly noteworthy as potential feedstocks. Their highly functionalized nature and oversupply means that they possess several economic benefits, compared with other low carbon building blocks.[4,5] However, the C−C bond cleavage is relatively facile in polyols due to the adjacent hydroxyl groups, which can hinder selective transformations and result in the formation of lower-value compounds, such as formic acid. Thus, the production of desirable high-value products from polyols, with stable selectivity and high conversion, remains a significant challenge. Among the C_1 to C_3 products that can be formed from the electrooxidation of polyols, glycolic acid is of specific interest to researchers. Indeed, glycolic acid, an oxidation derivative of glycerol and ethylene glycol, finds widespread applications in the bioplastic, medical, and cosmetic industries.[6,7] Currently, glycolic acid is primarily produced through microbial fermentation from pentose or hexose sugars.[8] However, these fermentation processes are typically time-intensive and require the involvement of several intricate separation procedures. These, in turn, pose limitations on the scalability of the technology and, thus, limit the advancement of applications for glycolic acid. Research on the production of glycolic acid through conventional thermocatalysis has been conducted, particularly by using glycerol and ethylene glycol as substrates. For instance, on Ag/Al_2O_3, 85% glycerol conversion with 57.1% selectivity to glycolic acid was achieved at 60 °C, 5 bar of O_2 pressure, 0.3 M glycerol, and NaOH/glycerol molar ratio of 4.[9] Under the same reaction conditions, a $Ag/Ce_{0.75}Zr_{0.25}O_2$ catalyst achieved over 98% conversion with 69% selectivity toward glycolic acid.[10] Cu/activated carbon displayed superior catalytic performance, achieving 98.6% glycerol conversion and 68.3% glycolic acid yield at 200 °C, 0.6 MPa O_2, and equal masses of glycerol to catalyst.[11] Further enhancement of

Received: January 22, 2024
Revised: June 24, 2024
Accepted: July 8, 2024

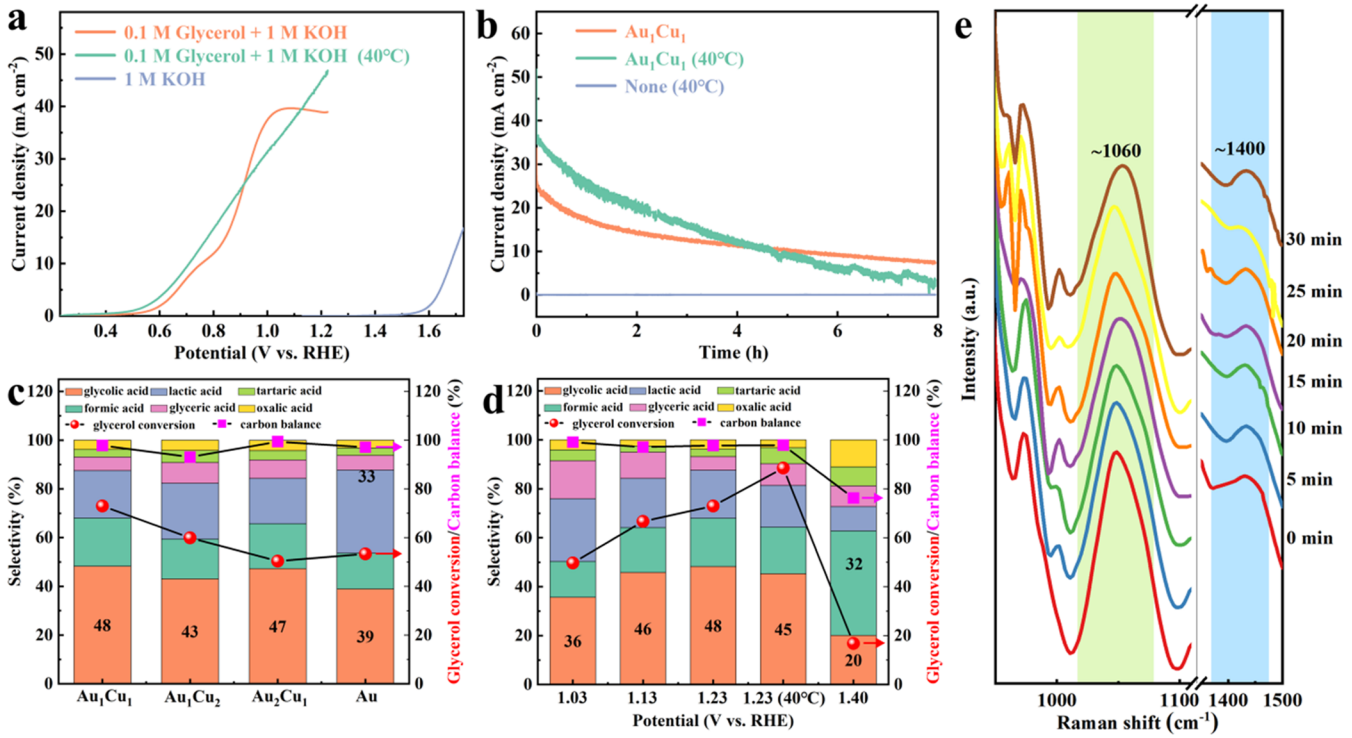

Figure 1. Anodic scan of the CV for Au_1Cu_1 with or without 0.1 M glycerol in 1 M KOH at a scan rate of 10 mV s^{-1} at room temperature and 40 °C (a), chronoamperograms with and without glycerol using Au_1Cu_1 at different temperatures at 1.23 V during 8 h (b), product selectivity and glycerol conversion for different catalysts after 8 h of reaction at 1.23 V (c), Product selectivity and glycerol conversion under the catalysis of Au_1Cu_1 after 8 h for different applied potentials (d); and *in situ* Raman measurement under the catalysis of Au_1Cu_1 at 1.40 V for 30 min (e); electrolyte: 1 M KOH and 0.1 M glycerol solution. All of the potentials are against reversible hydrogen electrode (RHE).

glycolic acid yield (up to 71.8%) was observed using Cu_1Mg_4 by replacing the spent catalyst with fresh catalyst after 4 h at 180 °C and 1 MPa O_2.[12] Zhang et al. developed a homogeneous iridium complex catalyst as the dehydrogenation catalyst, resulting in an 89.3% conversion of ethylene glycol with a glycolic acid yield of 70.8%.[13]

Electrocatalysis, driven by renewable energy sources, utilizes water as the source of oxygen and hydrogen in redox reactions, offering a green alternative to thermocatalytic approaches. To date, the selective electrocatalytic oxidation of polyols with precious metal catalysts (Au, Pd, Pt, and alloys thereof) has been extensively investigated. Au has, in particular, been determined to be a highly effective electrocatalyst for the partial oxidation of polyols under alkaline conditions. Xie et al.[14] observed that a Au/CP anode catalyst displayed promising behavior for the glycerol electrooxidation reaction (GEOR) at several electrochemical potentials. It exhibited an impressive 97% selectivity toward glyceric acid at 1.0 V, whereas at an elevated potential of 1.3 V, the reactant was predominantly converted into formic acid. Separately, Zhang et al.[15] assessed the impact of the applied potential and electrolyte concentration on the performance of Au electrocatalysts supported on carbon nanotubes. The authors noted that higher applied potentials were found to enhance glycolic acid formation, with an 85% selectivity toward glycolic acid, albeit with a modest glycerol conversion of only 34%. Kim et al.[16] also investigated the electrocatalytic properties of Au in these systems. Here, RA-Au materials were supported onto a Ni foam, which exhibited a remarkable selectivity for glycolic acid (41%), even at relatively high conversion (69%). However, the authors noted that the stability of the material was an issue as the kinetics was reduced over the course of the reaction. Previous studies have established that Au can catalyze both the cleavage of the C−C bond and the oxidation of the hydroxyl group, leading to the formation of several C_1−C_3 carboxylic acids.[17,18] While the research in this area has presented much promise, controlling the extent of the cleavage reactions and hydroxyl oxidation to a specific product remains a significant challenge. Herein, we report on the synthesis and application of a spheroidal hollow bimetallic Au_1Cu_1 catalyst, which is highly effective for the selective electrochemical conversion of polyols into C_2 carboxylic acids (glycolic acid and acetic acid). We delineate the influence of copper in shaping the hollow structure of the catalyst, augmenting the population of active sites, enhancing the strong adsorption of glycerol and its intermediates, and facilitating the absorption and transfer of hydroxide to Au. These factors collectively improve the overall activity and stability of the Au_1Cu_1 catalyst. Density functional theory (DFT) calculations revealed that the presence of Cu in $Au_1Cu_1(111)$ had an impact on the adsorption of glycerol and the dissociation of its intermediates into glycolic acid. The spheroidal hollow $Au_1Cu_1(111)$ alloy exhibits noteworthy catalytic activity, positioning it among the most effective catalysts documented to date. Additionally, cyclic chronoamperometry experiments demonstrate a high degree of stability for the catalyst.

RESULTS AND DISCUSSION

To begin our study, a series of monometallic and bimetallic catalysts containing Au and Cu were synthesized using a coreduction method, with varying ratios of the component metals. The bimetallic catalysts are labeled as Au_1Cu_1, Au_2Cu_1,

https://doi.org/10.1021/acscatal.4c00483
ACS Catal. 2024, 14, 11343−11351

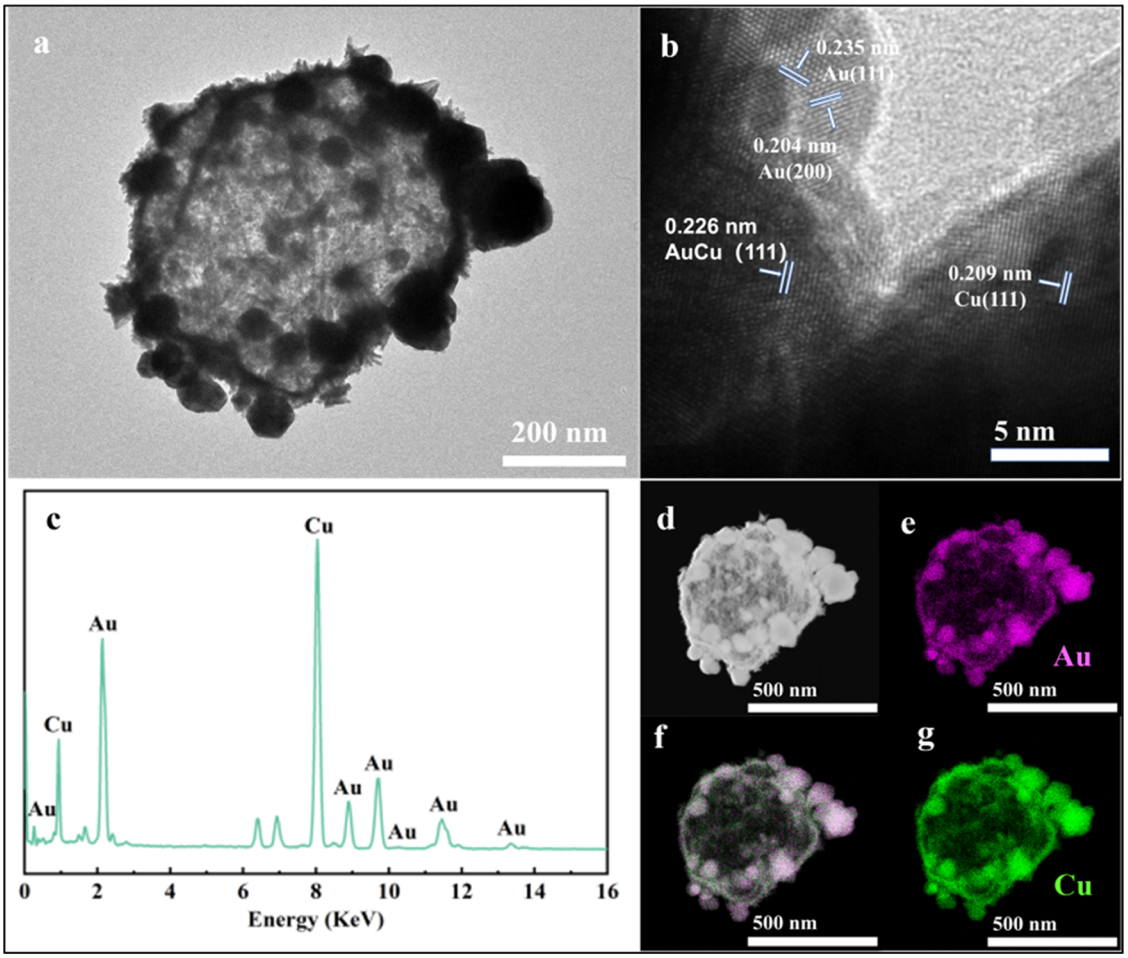

Figure 2. TEM (a) and HRTEM (b) images, EDX spectrum (c), and TEM−EDX mapping patterns (d−g) of the Au_1Cu_1 catalyst.

and Au_1Cu_2, with the subscript number representative of the ratio between the metals.

The electrochemical performances of the catalysts toward GEOR were first evaluated by cyclic voltammetry (CV), where each catalyst was assessed within a potential range spanning from 0.23 to 1.23 V in the presence of 0.1 M glycerol and 1 M KOH (Figures 1a and S3). The experimental outcomes indicate that the Au_1Cu_1 electrocatalyst exhibited the lowest onset potential (0.48 V) and the highest current density, reaching 39 mA cm^{-2} at 1.23 V, respectively. In contrast, the other AuCu bimetallic electrocatalysts displayed a lower current density of approximately 25 mA cm^{-2}, comparable to monometallic Au. The monometallic Cu electrocatalyst, on the other hand, showed negligible activity, exhibiting a considerably lower current density of about 2 mA cm^{-2}. Additionally, the reaction kinetics of the catalysts in glycerol were evaluated using Tafel slopes (Figure S4). AuCu alloys showed significantly lower Tafel slopes for glycerol oxidation compared to the pure Au catalyst, attributed to faster anodic catalytic kinetics, thus emphasizing the positive role of Cu in the catalysts.

Chronoamperometry tests were conducted on the catalysts at 1.23 V for 8 h (Figures 1b and S5), which were followed by measurements of glycerol conversion and product selectivity (Figure 1c and Table S1). The current density and glycerol conversion varied depending on the electrocatalyst used, in the order Cu < Au < Au_2Cu_1 < Au_1Cu_2 < Au_1Cu_1. Notably, the highest glycolic acid selectivity was achieved with the Au_1Cu_1 catalyst, reaching 48%.

The electrochemical surface areas (ECSAs) for each catalyst were subsequently determined, and the results, illustrated in Figures S6 and S7, revealed that Au_1Cu_1 exhibited the highest ECSA, i.e., 131 cm^2 g^{-1}. The monometallic Au and Au_2Cu_1 catalysts displayed similar ECSA values within the range of 54−56 cm^2 g^{-1}, while Au_1Cu_2 showed an ECSA of 82 cm^2 g^{-1}. These findings suggest that the presence of Cu significantly influences ECSA in the catalyst.

Subsequently, the influence of Cu on the structure of the bimetallic catalysts was explored. Transmission electron microscopy (TEM), high-resolution TEM (HRTEM), and TEM−energy dispersive X-ray (EDX) analyses were undertaken, and representative micrographs are presented in Figures 2a−g and S8−S10. The monometallic Au nanoparticles exhibit a dense hexagonal structure with an interplanar spacing of 0.235 nm indicative of the Au(111) crystal plane. Intriguingly, the introduction of Cu in the bimetallic catalysts induces a profound transformation in the morphology. Specifically, each bimetallic catalyst exhibits a spheroidal structure surrounded at its periphery by densely distributed nanoparticles of varying sizes and shapes. The core structure appears to be influenced by the Au/Cu ratio. For the Au_2Cu_1 catalyst, the core structure is dense and appears to be more enriched with copper. In contrast, with the Au_1Cu_1 and Au_1Cu_2 materials, the hollow structure of the core is more pronounced and Au and Cu alloying are clearly evidenced. This could explain why the

https://doi.org/10.1021/acscatal.4c00483
ACS Catal. 2024, 14, 11343−11351

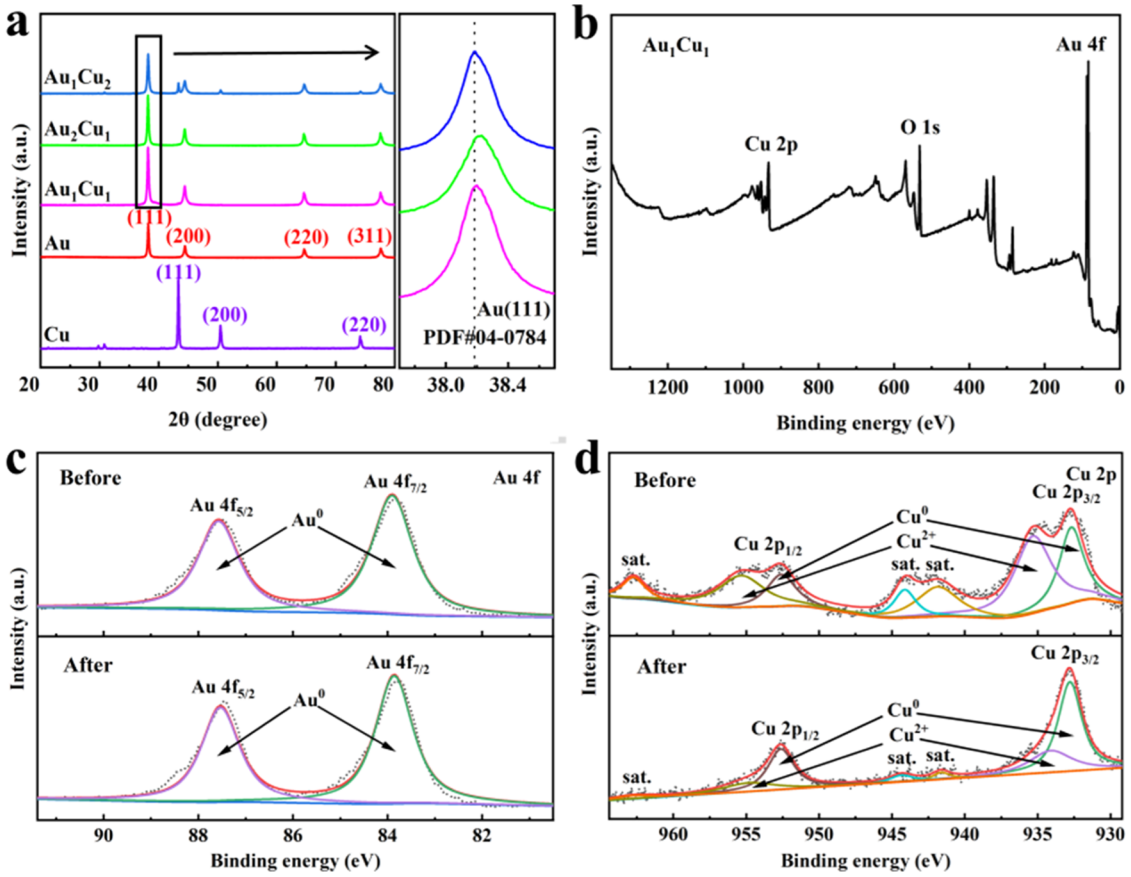

Figure 3. XRD patterns of the Au_1Cu_1, Au_2Cu_1, Au_1Cu_2, Au, and Cu (a), X-ray photoelectron spectra (XPS) of Au_1Cu_1 catalyst (b); XPS spectra of Au 4f (c) and Cu 2p (d) for the Au_1Cu_1 catalyst.

ECSA is higher for these two catalysts. The TEM−EDX mapping for the bimetallic catalysts indicates partial alloying in all cases, with a higher degree of alloying observed in the Au_1Cu_1 and Au_1Cu_2 catalysts. The analogous TEM experiments revealed that the Au_1Cu_1 material exhibited the smallest nanoparticle sizes at its periphery compared to the other bimetallic catalysts studied herein. These observations suggest that copper has a discernible effect on both the particle size and the spherical hollow structure of the catalysts, providing valuable insights into the intricate interplay between metal composition and catalyst morphology. Based on these results, it can be concluded that the spheroidal hollow morphology and the small particle sizes of the nanoparticles on the Au_1Cu_1 catalyst are the main factors contributing to its highest ECSA among the catalysts.

The catalyst structures were subsequently probed by X-ray diffraction (XRD) analysis, and the associated diffraction patterns are presented in Figure 3a. The AuCu catalysts exhibit four reflection peaks at 2θ = ca. 38.2, 44.4, 64.6, and 77.6°, which are characteristic of the (111), (200), (220), and (311) crystal planes of Au (JCPDS No. 04-0784), respectively. In addition, the reflection peak at ca. 2θ = 38.2° is indicative of the (111) crystal plane in Cu (JCPDS No. 04-0836). These lattice planes were confirmed by HRTEM (Figure 2b) of the Au_1Cu_1 material. There is a noticeable shift in the characteristic peak of the Au(111) plane toward a higher 2θ value with the bimetallic catalysts, which is characteristic of alloying. Interestingly, the extent of this shift is more pronounced and similar for both Au_1Cu_1 and Au_1Cu_2 materials, supporting the results acquired from the TEM−EDX mapping, where it was suggested that the degree of alloying was higher in these two electrocatalysts.

To gain further insight into the performance of the Au_1Cu_1 catalyst, the surface composition was probed by XPS, as illustrated in Figure 3b−d. Two distinctive peaks at ca. 83.9 and 87.6 eV are observed in the Au 4f region, which are indicative of Au^0 $4f_{5/2}$ and $4f_{7/2}$ (Figure 3c), respectively. On the contrary, the spectrum of the Cu 2p region has four distinct peaks at 932.1, 952.0, 935.2, and 954.1 eV (Figure 3d). The two peaks, located at 932.1 and 952.0 eV, are characteristic of Cu^0 $2p_{3/2}$ and $2p_{1/2}$ states, respectively. The remaining two peaks, at 935.2 and 954.1 eV, are indicative of the presence of Cu^{2+}. When compared to other examples in the literature,[19] it is evident that the Au^0 $4f_{5/2}$ and $4f_{7/2}$ peaks incur a positive shift of 0.3 and 0.4 eV, respectively. Conversely, the two characteristic peaks of Cu^0 exhibit a negative shift of 0.2 and 0.1 eV. Collectively, these observations provide further evidence of partial alloying between Au and Cu. Subsequently, further electrochemical testing was conducted with the Au_1Cu_1 catalyst at 40 °C and 1.23 V. The data revealed a reduction in the onset potential by approximately 100 mV and an increase in the current density, reaching 47 mA cm^{-2} at 1.23 V (Figure 1a). This value was 1.21 times higher than that observed at room temperature, which is likely to be attributable to the endothermic nature of the glycerol electrooxidation reaction.[20,21] The same reaction conditions were imposed without any catalyst, and no reactivity was observed (Figure 1b). These results highlight that higher reaction temperatures accelerate

https://doi.org/10.1021/acscatal.4c00483
ACS Catal. 2024, 14, 11343−11351

Table 1. Comparison of Glycerol Oxidation Performance in This Work and Previous Studies[a]

catalyst	electrolyte	onset potential vs. RHE	current density at 1.23 V vs. RHE (mA cm^{-2})	condition vs RHE	glycerol conversion (%)	glycolic acid selectivity (%)	refs
Au_1Cu_1(111)	0.1 M GLY + 1 M KOH	0.48 V	39	1.23 V RT	90	45	this work
$Rh_x\{Ni(OH)_2\}_y$/C	0.25 M GLY + 0.5 M KOH	1.05 V	4	1.50 V RT	23	6	24
$LaFe_{1-x}Co_xO_3$	1 M GLY + 1 M KOH	1.38 V	0	1.55 V RT	28	14	25
$ZnFe_xCo_{2-x}O_4$	0.5 M GLY + 1 M KOH	1.32 V	0	1.62 V RT	36	14	26
$NiSe_2$	0.05 M GLY + 0.1 M $NaHSO_4/Na_2SO_4$			0.60 V RT	55	3	27
Ni_xAu_{1-x}	0.1 M GLY + 1 M KOH	1.23 V	0	1.55 V 50 °C	62	9	28
RA-Au	0.1 M GLY + 1 M KOH	0.80 V	120	1.0 V RT	72	47	16
$CuCo_2O_4$	0.1 M GLY + 0.1 M KOH	1.06 V	5	1.14 V RT	80	3	29
Pt-CeO_2/CNT	0.1 M GLY + 1 M KOH	0.45 V		0.90 V 60 °C	87	10	30
Pt_{1-x}-Bi_x/TiN HNWs/CC	0.05 M GLY + 1 M KOH		20	0.85 V RT	87	1	31
NiCo hydroxide	0.1 M GLY + 1 M KOH	1.20 V	5	1.62 V RT	87	4	32

[a]Key: room temperature (RT), glycerol (GLY).

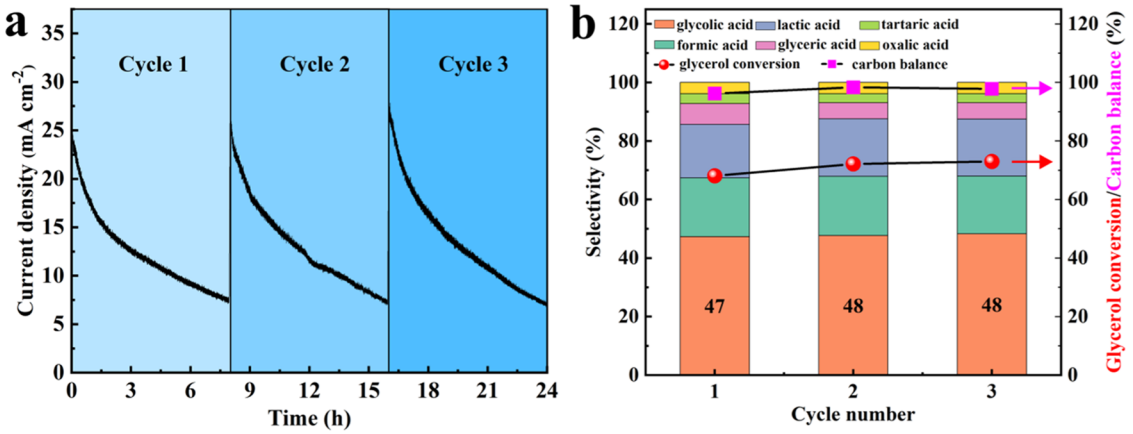

Figure 4. Cyclic chronoamperograms of Au_1Cu_1 in an initial 1 M KOH and 0.1 M glycerol at 1.23 V for 24 h (3 times 8 h) (a); product selectivity and glycerol conversion in the corresponding cycle (b). All of the data are against RHE.

the entire continuous reaction rate, without altering the energy barriers between reactions. A control experiment was conducted in the absence of glycerol over the Au_1Cu_1 catalyst, and there was no evidence to suggest that the oxygen evolution reaction (OER) was involved in the electrocatalytic process (Figure 1a).

Next, the performance of the Au_1Cu_1 catalyst was evaluated at different potentials, from 1.03 to 1.40 V, for 8 and 16 h (Figures 1d and S11). After 8 h, the highest catalytic activity was observed at 1.23 V, achieving a remarkable 73% glycerol conversion and 48% selectivity toward glycolic acid (Table S2). At 40 °C, the performance increased further with glycerol conversion reaching approximately 90%, representing a 16% increase compared to that exhibited under ambient conditions (Table S3). However, it should be noted that the selectivity to glycolic acid decreased slightly to 45% under these conditions. At lower potentials, the carbon balances observed are all close to 100%, indicating that the final amount of carbon dioxide produced is very low, as this was not quantified in the reactions due to the low amount produced. Upon increasing the applied potential to 1.40 V, the mass balance diminished to 77%, suggesting that considerably carbon dioxide would be produced. In order to verify this hypothesis, *in situ* Raman spectroscopy was performed, and the results are presented in Figure 1e. Over extended reaction durations, the gradual accumulation of carbonate causes a slight shift in the characteristic peaks around 1060 and 1400 cm^{-1}, which respectively correspond to the symmetric and asymmetric stretching vibrations of the carbonate ions.[22,23] The results suggest that at 1.40 V, there is a higher likelihood of C−C bond cleavage, resulting in the formation of carbonate, which can lead to the formation of carbon dioxide. Besides, the glycerol conversion was notably lower (at 17%), which was accompanied by a substantial shift in the product distribution, as formic acid became the primary product in the liquid phase (Figure 1d).

After 16 h of electrocatalysis at 1.23 V, glycerol conversion reached 90% and the selectivity reached 45% (Figure S11d), establishing it as one of the most efficient catalysts reported for GEOR to date (Table 1). It should be noted that the theoretical yield for glycolic acid from glycerol is 66.7% as one glycerol molecule produces one glycolic acid molecule. Chronoamperometry experiments conducted for 16 h at 1.23 V suggest that the catalyst may deactivate over the course of the reaction. To elucidate the source of this deactivation, cyclic chronoamperometry measurements were undertaken, involving the replenishment of a new electrolyte solution of 1 M KOH with 0.1 M glycerol every 8 h for 3 cycles. The results of these

https://doi.org/10.1021/acscatal.4c00483
ACS Catal. 2024, 14, 11343−11351

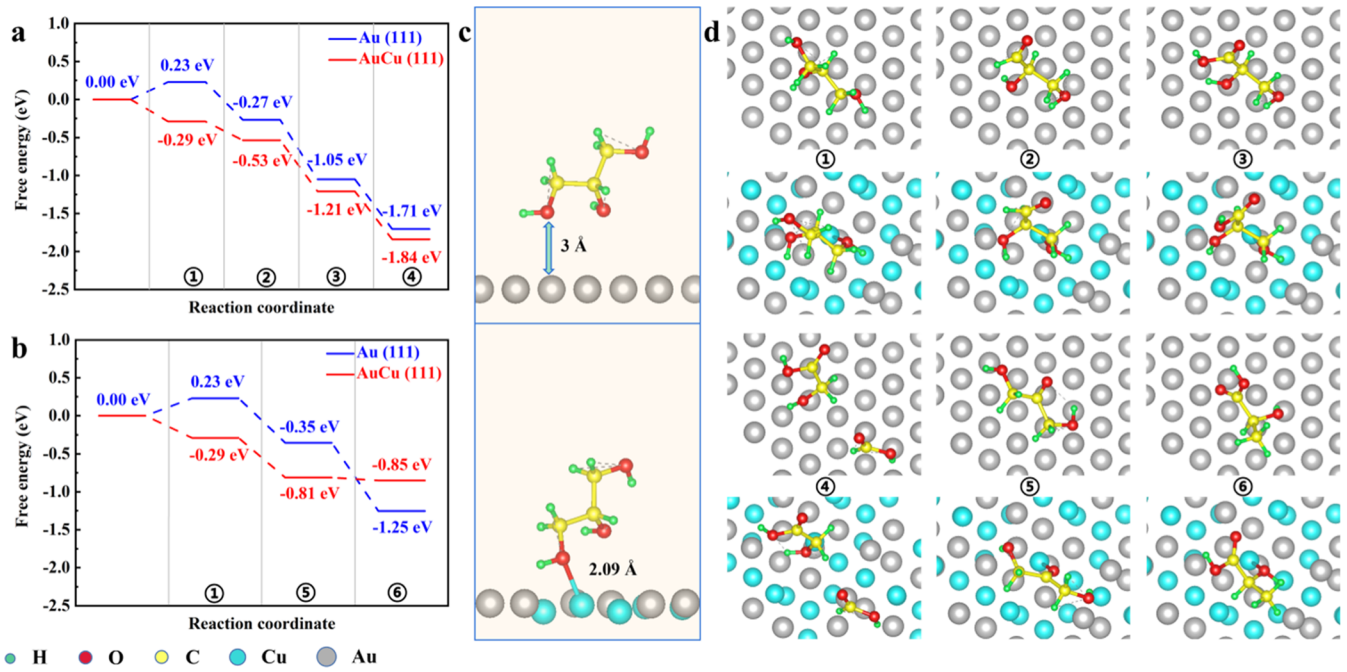

Figure 5. Free-energy diagrams of the reaction paths of glycerol adsorption in the formation of (a) glycolic acid and (b) lactic acid on Au(111) and AuCu(111) crystalline surfaces. Glycerol configuration on Au(111) and AuCu(111) (c). Top view of the model optimized for glycerol adsorption on Au(111) and AuCu(111) (d). White, brown, red, blue, and golden yellow represent hydrogen, carbon, oxygen, copper, and gold, respectively.

measurements are presented in Figure 4. During the initial 8 h cycle, the current density decreased. Three cycles indicated that the sustained decrease in reaction current density primarily stems from the consumption of electrolyte solution rather than a decline in electrocatalyst activity. The starting current, glycerol conversion, and product distribution in each cycle remained largely unchanged compared with the first cycle. The high activity exhibited by the Au_1Cu_1 catalyst in the GEOR could be due to the surface adsorption of hydroxides on the Au in alkaline environments, forming $Au(OH)_{ads}$. This, in turn, lowers the O−H bond dissociation barriers and could allow Au to actively participate in alcohol oxidation reactions.[33,34] In the aim to validate this hypothesis, we have conducted cyclic voltammetry over Au and Au_1Cu_1, in the absence of glycerol, in 0.1 M KOH electrolyte solution. The Au−OH*[35] signal peak near 0.8 V was significantly enhanced for the Au_1Cu_1 catalyst compared to pure Au (Figure S12). This enhancement could be attributed to the strong adsorption of hydroxides by copper oxide, which are then transferred to the Au surface.[36,37]

In the aim to have more insight into the role of copper in the Au_1Cu_1 catalyst, electrochemical *in situ* Fourier transform infrared spectroscopy (FTIR) was employed to study the reaction pathway of glycerol on the Au_1Cu_1 and Au catalysts, during a 30 min reaction at 1.23 V vs RHE (Figures S13−S15 and Table S4).[38] The analysis of the products after 30 min was also conducted, and the data are reported in Tables S5 and S6, clearly demonstrating distinct behaviors between the bimetallic Au_1Cu_1 and monometallic Au catalysts. While most intermediates and products are detectable from the beginning of the FTIR measurements, significant differences can be highlighted between the two catalysts. The first notable difference is in peak intensity in the FTIR spectra, which is much higher for Au_1Cu_1 compared to Au, suggesting stronger adsorption of glycerol and its intermediates on Au_1Cu_1. This observation aligns with the DFT data. Furthermore, in the absence of copper, Au tends to promote the production of lactic acid. The formation of lactic acid is known to proceed through a base-catalyzed dehydration of dihydroxyacetone and glyceraldehyde, followed by a Cannizzaro rearrangement.[39] The larger amount of lactic acid observed on monometallic Au could be explained by the weak adsorption of dihydroxyacetone/glyceraldehyde, which rapidly undergoes dehydration in the solution. In contrast, for Au_1Cu_1, the stronger adsorption of these intermediates could accelerate the formation of glyceric acid, glycolic acid, and formic acid.

Another interesting observation is the absence of tartronic acid in the solution, after 30 min reaction, for Au_1Cu_1, despite its presence in the FTIR spectra. This again suggests a strong adsorption of this intermediate on Au_1Cu_1, whereas its adsorption is weaker on Au, as evidenced by the presence of tartronic acid in the solution. We hypothesize that the strong adsorption of tartronic acid could lead to its cleavage and could explain the higher amounts of glycolic acid and formic acid observed with the Au_1Cu_1 catalyst (see Schemes S1 and S2), compared to Au.[40]

DFT calculations were subsequently employed to assess the surface mechanisms taking place. Free-energy diagrams of the primary reaction pathways of glycerol on AuCu(111) and Au(111) are presented in Figure 5a,b. A bird's-eye view of the optimized models for glycerol adsorption on the AuCu(111) and Au(111) is displayed in Figure 5c,d. Clearly, the adsorption energy of glycerol on AuCu(111) (−0.29 eV) is lower than that of Au(111) (0.23 eV), indicating that there is a stronger adsorption capability for glycerol on the AuCu(111) surface. On Au(111), the adsorption of glycerol molecules is weak, with glycerol molecules positioned approximately 3 Å from the surface. Upon introduction of Cu into the catalyst to form AuCu(111), glycerol molecules adsorb on the surface in an upright configuration, forming Cu−O bonds with a length of 2.09 Å, thereby facilitating the dissociation of intermediates to form glycolic acid. On one hand, even when considering

https://doi.org/10.1021/acscatal.4c00483
ACS Catal. 2024, 14, 11343−11351

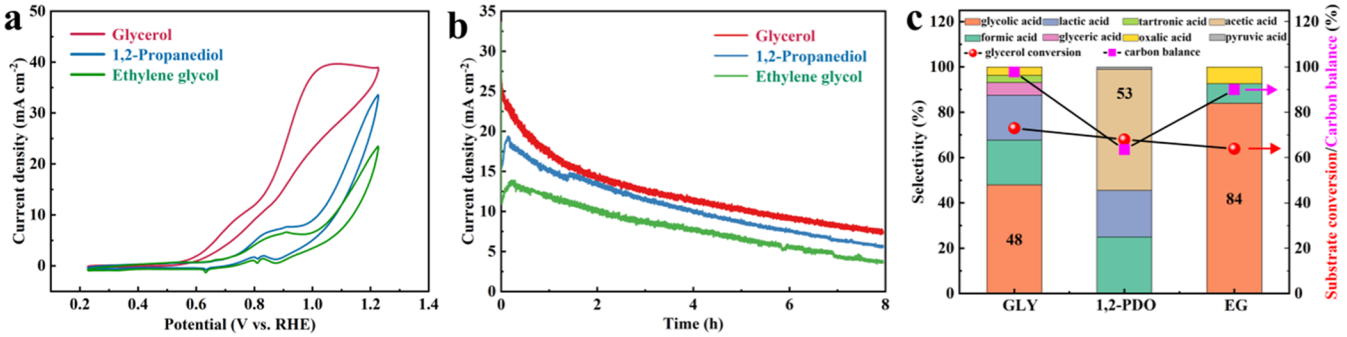

Figure 6. CVs (a), chronoamperograms (b), and product selectivity and substrate conversion (c) in electrolyte with 1 M KOH and 0.1 M glycerol, 1,2-propanediol or ethylene glycol at 1.23 V, respectively. All of the data are against RHE.

intermediate reaction pathways, the adsorption of the glycolic acid on the AuCu(111) alloy is thermodynamically more stable compared to the adsorption of glycolic acid on the pure Au(111) surface (0.13 eV). In contrast, for the pathway leading to lactic acid formation on the catalyst surface, the adsorption of lactic acid on Au(111) is thermodynamically more stable than the adsorption of lactic acid on the Au(111) alloy (0.40 eV). This suggests that Au(111) generates more lactic acid on its surface, while AuCu(111) forms more glycolic acid on its surface. The computational results align well with the experimental observations and emphasize the crucial role of copper in enhancing the adsorption capacity and performance of Au_1Cu_1.

To assess the generality of the effect, Au_1Cu_1 was subsequently applied as a catalyst for the electrocatalytic oxidation of 1,2-propanediol and ethylene glycol. The CVs presented in Figure 6a were conducted with an electrolyte solution of 1 M KOH and/or 0.1 M glycerol, 1,2-propanediol, or ethylene glycol. With the Au_1Cu_1 electrocatalyst, a similarly high activity at 1.23 V was observed for the oxidation of 1,2-propanediol or ethylene glycol, yielding current densities of 33 and 23 mA cm^{-2}, respectively. After 8 h of reaction (Figure 6b,c and Table S7) the 1,2-propanediol undergoes substantial conversion of 68%. Acetic acid and formic acid were determined to be the primary and secondary byproducts, exhibiting selectivities of 53% and 25%, respectively. The product distribution data revealed that the Au_1Cu_1 catalyst harnesses the cleavage of C−C bonds in 1,2-propanediol, especially between the α and β carbon atoms, thereby resulting in the formation of acetic acid. This observation is in stark contrast with previous studies conducted using Pt/C or Au/C catalysts, where the primary products were determined to be lactic acid or pyruvic acid.[41,42] This discrepancy can be attributed to the ability of Au_1Cu_1(111) to adsorb both the primary and secondary carbon atoms simultaneously during these reactions.[43] Additionally, under applied potentials exceeding 0.90 V, Au promotes the disruption of C−C bonds, resulting in the formation of C_1 products.[44]

Under identical experimental conditions, when ethylene glycol was used as the substrate, the conversion rate reached 64%, with glycolic acid as the major product exhibiting a selectivity of 84%. Small amounts of formic acid and oxalic acid were observed as byproducts. Compared to the product distribution in glycerol and 1,2-propanediol oxidation, ethylene glycol underwent fewer C−C bond cleavages when subjected to the Au_1Cu_1 alloy catalysts. Considering that the oxidation reactions of glycerol and 1,2-propanediol primarily yield glycolic acid and acetic acid as major products, this product distribution aligns with the anticipated outcomes. This suggests that the electrocatalytic oxidation of ethylene glycol is predominantly conducive to the oxidation of hydroxyl groups rather than C−C cleavage into formic acid.

CONCLUSIONS

A hollow Au_1Cu_1 electrocatalyst has proven to be highly selective for the electrocatalytic valorization of polyols (glycerol, 1,2-propanediol, and ethylene glycol) into glycolic acid and acetic acid. In a 1 M KOH solution containing 0.1 M glycerol, the glycerol conversion rate and glycolic acid selectivity reached 90 and 45%, respectively, after 16 h of reaction at a fixed potential of 1.23 V vs RHE. Elevating the reaction temperature to 40 °C allowed glycerol conversion to reach the same level as the 16 h of electrolysis in just half the time. In comparison to an analogous Au catalyst, the Au_1Cu_1 catalyst demonstrated a superior and more consistent selectivity for glycolic acid at intermediate potentials of 1.03, 1.13, and 1.23 V. After three consecutive 8 h electrolysis cycles at 1.23 V, the catalyst exhibited remarkable stability, with minimal changes in glycerol conversion and glycolic acid selectivity. Physicochemical characterizations and kinetic and mechanistic studies highlighted the significant role of copper in enhancing the number of exposed active sites for the reactants, influencing the size of nanoparticles, and also improving the capacity of Au to adsorb more $^-$OH leading to better activity and stability. DFT analysis and electrochemical *in situ* FTIR highlighted the role of copper in facilitating both reactant and intermediate strong adsorption, leading to high selective conversion to glycolic acid.

ASSOCIATED CONTENT

Supporting Information

The Supporting Information is available free of charge at https://pubs.acs.org/doi/10.1021/acscatal.4c00483.

Electrochemical testing; details of the Faraday efficiency calculations; product analysis; CV results; ECSA calculation; supporting characterization for catalysts and reaction system; and specific activity data of each catalyst (PDF)

AUTHOR INFORMATION

Corresponding Authors

Ouardia Akdim − *Max Planck-Cardiff Centre on the Fundamentals of Heterogeneous Catalysis FUNCAT, Cardiff Catalysis Institute, School of Chemistry, Cardiff University, Translational Research Hub, Cardiff CF24 4HQ, U.K.;*

https://doi.org/10.1021/acscatal.4c00483
ACS Catal. 2024, 14, 11343−11351

orcid.org/0000-0003-3915-7681; Email: Akdimo@cardiff.ac.uk

Graham J. Hutchings − *Max Planck-Cardiff Centre on the Fundamentals of Heterogeneous Catalysis FUNCAT, Cardiff Catalysis Institute, School of Chemistry, Cardiff University, Translational Research Hub, Cardiff CF24 4HQ, U.K.;* orcid.org/0000-0001-8885-1560; Email: Hutchings@cardiff.ac.uk

Authors

Lingqin Shen − *School of Chemistry and Chemical Engineering, Jiangsu University, Zhenjiang 212013, China; Max Planck-Cardiff Centre on the Fundamentals of Heterogeneous Catalysis FUNCAT, Cardiff Catalysis Institute, School of Chemistry, Cardiff University, Translational Research Hub, Cardiff CF24 4HQ, U.K.;* orcid.org/0000-0001-8267-2959

Luyao Sun − *School of Chemistry and Chemical Engineering, Jiangsu University, Zhenjiang 212013, China*

Mark Douthwaite − *Max Planck-Cardiff Centre on the Fundamentals of Heterogeneous Catalysis FUNCAT, Cardiff Catalysis Institute, School of Chemistry, Cardiff University, Translational Research Hub, Cardiff CF24 4HQ, U.K.*

Stuart Taylor − *Max Planck-Cardiff Centre on the Fundamentals of Heterogeneous Catalysis FUNCAT, Cardiff Catalysis Institute, School of Chemistry, Cardiff University, Translational Research Hub, Cardiff CF24 4HQ, U.K.;* orcid.org/0000-0002-1933-4874

Complete contact information is available at: https://pubs.acs.org/10.1021/acscatal.4c00483

Notes

The authors declare no competing financial interest.

■ ACKNOWLEDGMENTS

The authors would like to thank the Max Planck Centre for Fundamental Heterogeneous Catalysis (FUNCAT) for financial support.

■ REFERENCES

(1) Monteiro, M. R.; Kugelmeier, C. L.; Pinheiro, R. S.; Batalha, M. O.; da Silva César, A. Glycerol from biodiesel production: Technological paths for sustainability. *Renewable Sustainable Energy Rev.* **2018**, *88*, 109−122.

(2) Holade, Y.; Tuleushova, N.; Tingry, S.; Servat, K.; Napporn, T. W.; Guesmi, H.; Cornu, D.; Kokoh, K. B. Recent advances in the electrooxidation of biomass-based organic molecules for energy, chemicals and hydrogen production. *Catal. Sci. Technol.* **2020**, *10*, 3071−3112.

(3) Lv, H.; Xiao, Z.; Zhai, S.; Wang, X.; Hao, J.; Tong, Y.; An, Q. Ni3S2 nanoparticles encapsulated in S-doped biomass-derived hierarchically porous carbon as an advanced electrode for excellent hybrid supercapacitors performance. *Ind. Crops Prod.* **2023**, *194*, No. 116320.

(4) Mane, R.; Jeon, Y.; Rode, C. A review on non-noble metal catalysts for glycerol hydrodeoxygenation to 1,2-propanediol with and without external hydrogen. *Green Chem.* **2022**, *24*, 6751−6781.

(5) Liu, Y.; Rempel, G. L.; Ng, F. T. T. Kinetic study of Pd-Promoting effect on Cu/ZnO/Al2O3 catalyst for glycerol hydrogenolysis to produce 1,2-propanediol at low hydrogen pressure. *Biomass* **2022**, *2*, 27−45.

(6) Bagheri, S.; Julkapli, N. M.; Yehye, W. A. Catalytic conversion of biodiesel derived raw glycerol to value added products. *Renewable Sustainable Energy Rev.* **2015**, *41*, 113−127.

(7) Li, T.; Harrington, D. A. An overview of glycerol electrooxidation mechanisms on Pt, Pd and Au. *ChemSusChem* **2021**, *14*, 1472−1495.

(8) Salusjärvi, L.; Havukainen, S.; Koivistoinen, O.; Toivari, M. Biotechnological production of glycolic acid and ethylene glycol: current state and perspectives. *Appl. Microbiol. Biotechnol.* **2019**, *103*, 2525−2535.

(9) Skrzyńska, E.; Zaid, S.; Addad, A.; Girardon, J. S.; Capron, M.; Dumeignil, F. Performance of Ag/Al2O3 catalysts in the liquid phase oxidation of glycerol − effect of preparation method and reaction conditions. *Catal. Sci. Technol.* **2016**, *6*, 3182−3196.

(10) Tavera Ruiz, C. P.; Dumeignil, F.; Capron, M. Catalytic production of glycolic acid from glycerol oxidation: an optimization using response surface methodology. *Catalysts* **2021**, *11*, No. 257, DOI: 10.3390/catal11020257.

(11) Liao, S.; Tian, Q.; Xiao, Y.; Qin, D.; Li, J.; Hu, C. Glycerol valorization towards glycolic acid production over Cu-Based biochar catalyst. *ChemSusChem* **2022**, *15*, No. e202201537, DOI: 10.1002/cssc.202201537.

(12) Zhan, Y.; Hou, W.; Li, G.; Shen, Y.; Zhang, Y.; Tang, Y. Oxidant-Free transformation of ethylene glycol toward glycolic acid in water. *ACS Sustainable Chem. Eng.* **2019**, *7*, 17559−17564.

(13) Xu, S.; Xiao, Y.; Zhang, W.; Liao, S.; Yang, R.; Li, J.; Hu, C. Relay catalysis of copper-magnesium catalyst on efficient valorization of glycerol to glycolic acid. *Chem. Eng. J.* **2022**, *428*, No. 132555, DOI: 10.1016/j.cej.2021.132555.

(14) Xie, Y.; Sun, L.; Pan, X.; Zhou, Z.; Zheng, Y.; Yang, X.; Zhao, G. Carbon paper supported gold nanoflowers for tunable glycerol electrooxidation boosting efficient hydrogen evolution. *Carbon* **2023**, *203*, 88−96.

(15) Zhang, Z.; Xin, L.; Qi, J.; Wang, Z.; Li, W. Selective electroconversion of glycerol to glycolate on carbon nanotube supported gold catalyst. *Green Chem.* **2012**, *14*, 2150 DOI: 10.1039/c2gc35505a.

(16) Kim, D.; Oh, L. S.; Tan, Y. C.; Song, H.; Kim, H. J.; Oh, J. Enhancing glycerol conversion and selectivity toward glycolic acid via precise nanostructuring of electrocatalysts. *ACS Catal.* **2021**, *11*, 14926−14931.

(17) Bott-Neto, J. L.; Garcia, A. C.; Oliveira, V. L.; de Souza, N. E.; Tremiliosi-Filho, G. Au/C catalysts prepared by a green method towards C3 alcohol electrooxidation: A cyclic voltammetry and in situ FTIR spectroscopy study. *J. Electroanal. Chem.* **2014**, *735*, 57−62.

(18) Zhou, Y.; Shen, Y.; Luo, X. Optimizing the activity and selectivity of glycerol oxidation over core-shell electrocatalysts. *J. Catal.* **2020**, *381*, 130−138.

(19) Li, P.; Liu, L.; An, W.; Wang, H.; Guo, H.; Liang, Y.; Cui, W. Ultrathin porous g-C3N4 nanosheets modified with AuCu alloy nanoparticles and C-C coupling photothermal catalytic reduction of CO to ethanol. *Appl. Catal., B* **2020**, *266*, No. 118618, DOI: 10.1016/j.apcatb.2020.118618.

(20) Geraldes, A. N.; da Silva, D. F.; e Silva, L. G. d. A.; Spinacé, E. V.; Neto, A. O.; dos Santos, M. C. Binary and ternary palladium based electrocatalysts for alkaline direct glycerol fuel cell. *J. Power Sources* **2015**, *293*, 823−830.

(21) Lee, C. S.; Aroua, M. K.; Wan Daud, W. A.; Cognet, P.; Pérès, Y.; Ajeel, M. A. Selective electrochemical conversion of glycerol to glycolic acid and lactic acid on a mixed Carbon-Black activated carbon electrode in a single compartment electrochemical cell. *Front. Chem.* **2019**, *7*, No. 110, DOI: 10.3389/fchem.2019.00110.

(22) Luo, W.; Tian, H.; Li, Q.; Meng, G.; Chang, Z.; Chen, C.; Shen, R.; Yu, X.; Zhu, L.; Kong, F.; Cui, X.; Shi, J. Controllable electron distribution reconstruction of spinel NiCo2O4 boosting glycerol oxidation at elevated current density. *Adv. Funct. Mater.* **2023**, *34*, No. 2306995, DOI: 10.1002/adfm.202306995.

(23) Zhou, Y.; Slater, T. J. A.; Luo, X.; Shen, Y. A versatile single-copper-atom electrocatalyst for biomass valorization. *Appl. Catal., B* **2023**, *324*, No. 122218, DOI: 10.1016/j.apcatb.2022.122218.

(24) Xavier, F. F. S.; Cunha, A. C.; Napporn, T. W.; Olivi, P. Replacing oxygen evolution reaction by glycerol electrooxidation on

Rh modified Ni(OH)2/C for energy-efficient hydrogen production. *Int. J. Hydrogen Energy* **2023**, *48*, 31091−31100.
(25) Brix, A. C.; Dreyer, M.; Koul, A.; Krebs, M.; Rabe, A.; Hagemann, U.; Varhade, S.; Andronescu, C.; Behrens, M.; Schuhmann, W.; Morales, D. M. Structure-Performance relationship of LaFe1-xCoxO3 electrocatalysts for oxygen evolution, isopropanol oxidation, and glycerol oxidation. *ChemElectroChem* **2022**, *9*, No. e202200092, DOI: 10.1002/celc.202200092.
(26) Wan, H.; Dai, C.; Jin, L.; Luo, S.; Meng, F.; Chen, G.; Duan, Y.; Liu, C.; Xu, Q.; Lu, J.; Xu, Z. Electro-Oxidation of glycerol to High-Value-Added C1−C3 products by Iron-Substituted spinel zinc cobalt oxides. *ACS Appl. Mater. Interfaces* **2022**, *14*, 14293−14301.
(27) Sheng, H.; Janes, A. N.; Ross, R. D.; Hofstetter, H.; Lee, K.; Schmidt, J. R.; Jin, S. Linear paired electrochemical valorization of glycerol enabled by the electro-Fenton process using a stable NiSe2 cathode. *Nat. Catal.* **2022**, *5*, 716−725.
(28) Houache, M. S. E.; Shubair, A.; Sandoval, M. G.; Safari, R.; Botton, G. A.; Jasen, P. V.; González, E. A.; Baranova, E. A. Influence of Pd and Au on electrochemical valorization of glycerol over Ni-rich surfaces. *J. Catal.* **2021**, *396*, 1−13.
(29) Han, X.; Sheng, H.; Yu, C.; Walker, T. W.; Huber, G. W.; Qiu, J.; Jin, S. Electrocatalytic oxidation of glycerol to formic acid by CuCo2O4 spinel oxide nanostructure catalysts. *ACS Catal.* **2020**, *10*, 6741−6752.
(30) Li, J.; Li, Z.; Zheng, Z.; Zhang, X.; Zhang, H.; Wei, H.; Chu, H. Tuning the Product selectivity toward the high yield of glyceric acid in Pt−CeO2/CNT electrocatalyzed oxidation of glycerol. *ChemCatChem* **2022**, *14*, No. e202200509, DOI: 10.1002/cctc.202200509.
(31) Liu, L.; Liu, B.; Xu, X.; Jing, P.; Zhang, J. Heterogeneous Pt-Bi hybrid nanoparticle decorated self-standing hollow TiN nanowire as an efficient catalyst for glycerol electrooxidation. *J. Power Sources* **2022**, *543*, No. 231836, DOI: 10.1016/j.jpowsour.2022.231836.
(32) He, Z.; Hwang, J.; Gong, Z.; Zhou, M.; Zhang, N.; Kang, X.; Han, J. W.; Chen, Y. Promoting biomass electrooxidation via modulating proton and oxygen anion deintercalation in hydroxide. *Nat. Commun.* **2022**, *13*, No. 3777, DOI: 10.1038/s41467-022-31484-0.
(33) Rodriguez, P.; Kwon, Y.; Koper, M. T. M. The promoting effect of adsorbed carbon monoxide on the oxidation of alcohols on a gold catalyst. *Nat. Chem.* **2012**, *4*, 177−182.
(34) Verma, A. M.; Laverdure, L.; Melander, M. M.; Honkala, K. Mechanistic origins of the pH dependency in Au-Catalyzed glycerol Electro-oxidation: insight from First-Principles calculations. *ACS Catal.* **2022**, *12*, 662−675.
(35) Yan, Y.; Zhou, H.; Xu, S.-M.; Yang, J.; Hao, P.; Cai, X.; Ren, Y.; Xu, M.; Kong, X.; Shao, M.; Li, Z.; Duan, H. Electrocatalytic upcycling of biomass and plastic wastes to biodegradable polymer monomers and hydrogen fuel at high current densities. *J. Am. Chem. Soc.* **2023**, *145*, 6144−6155.
(36) Pittayaporn, N.; Therdthianwong, A.; Therdthianwong, S. Au/C catalysts promoted with Ni for glycerol electrooxidation in alkaline media. *J. Appl. Electrochem.* **2018**, *48*, 251−262.
(37) Li, Z.; Yan, Y.; Xu, S.-M.; Zhou, H.; Xu, M.; Ma, L.; Shao, M.; Kong, X.; Wang, B.; Zheng, L.; Duan, H. Alcohols electrooxidation coupled with H2 production at high current densities promoted by a cooperative catalyst. *Nat. Commun.* **2022**, *13*, No. 147, DOI: 10.1038/s41467-021-27806-3.
(38) Mahoney, E. G.; Sheng, W.; Cheng, M.; Lee, K. X.; Yan, Y.; Chen, J. G. Analyzing the electrooxidation of ethylene glycol and glucose over platinum-modified gold electrocatalysts in alkaline electrolyte using in-situ infrared spectroscopy. *J. Power Sources* **2016**, *305*, 89−96.
(39) Yelekli Kirici, E.; Angizi, S.; Higgins, D. A universal roadmap for quantification of glycerol electrooxidation products using proton nuclear magnetic spectroscopy (1H NMR). *ACS Catal.* **2024**, *14*, 9328−9341.
(40) Oh, L. S.; Han, J.; Lim, E.; Kim, W. B.; Kim, H. J. PtCu nanoparticle catalyst for electrocatalytic glycerol oxidation: how does the PtCu affect to glycerol oxidation reaction performance by changing pH conditions? *Catalysts* **2023**, *13*, No. 892, DOI: 10.3390/catal13050892.
(41) Chadderdon, D. J.; Xin, L.; Qi, J.; Brady, B.; Miller, J. A.; Sun, K.; Janik, M. J.; Li, W. Selective oxidation of 1,2-propanediol in alkaline Anion-Exchange membrane electrocatalytic flow reactors: experimental and DFT investigations. *ACS Catal.* **2015**, *5*, 6926−6936.
(42) Xi, N.; Zang, Y.; Sun, X.; Yu, J.; Johnsson, M.; Dai, Y.; Sang, Y.; Liu, H.; Yu, X. Polyhedral coordination determined Co-O activity for electrochemical oxidation of biomass alcohols. *Adv. Energy Mater.* **2023**, *13*, No. 2301572.
(43) Mello, G. A. B.; Busó-Rogero, C.; Herrero, E.; Feliu, J. M. Glycerol electrooxidation on Pd modified Au surfaces in alkaline media: Effect of the deposition method. *J. Chem. Phys.* **2019**, *150*, No. 041703, DOI: 10.1063/1.5048489.
(44) Alaba, P. A.; Lee, C. S.; Abnisa, F.; Aroua, M. K.; Cognet, P.; Pérès, Y.; Wan Daud, W. M. A. A review of recent progress on electrocatalysts toward efficient glycerol electrooxidation. *Rev. Chem. Eng.* **2021**, *37*, 779−811.